Supporting Information

Kim et al. 10.1073/pnas.1707745115

SI Materials and Methods

Inelastic Neutron Scattering. Inelastic neutron scattering measurements were performed on a single crystal of silicon of 99.999% purity that was highly oriented ($<2^\circ$), purchased from Virginia Semiconductor, Inc. The [110] oriented single crystal was further machined into a cylinder of 3.8 cm in height, 2.54 cm in outer diameter, and a 1.59-cm inner diameter to minimize multiple scattering. The crystal was suspended in an aluminum holder and then mounted into a closed-cycle helium refrigerator for the 100 and 200 K measurements, and a similar holder made from niobium was mounted into a low-background electrical resistance vacuum furnace for measurements at 300, 900, 1,200, and 1,500 K. For all measurements, the incident energy was 97.5 meV, and an oscillating radial collimator was used to reduce background and multiple scattering (38, 49).

The time-of-flight neutron data included multiple datasets from 200 rotations in increments of 0.5° about the vertical [110] axis, reduced to create the 4D $S(q,\varepsilon)$ (50, 51). A secondary data reduction process consisted of folding the entire $S(q,\varepsilon)$ dataset into an irreducible wedge in the first Brillouin zone. Nonlinear offsets of the q grid were corrected by fitting typically 50 in situ Bragg diffractions in an energy transfer range of $\Delta\varepsilon = \pm 4$ meV by a transformation to the positions of the theoretical diffraction peaks for a diamond cubic structure. The multiphonon scattering was then subtracted, and the data were "folded back" and corrected for the phonon creation thermal factor (39).

The multiphonon scattering was determined with q dependence through the incoherent approximation and calculated from Eq. **S1** (39),

$$S_{n>1}(\mathbf{q},\varepsilon) = \sum_{n=2}^{10} e^{-2W}\frac{(2W)^n}{n!} A_1 \circledast A_{n-1}, \qquad \textbf{[S1]}$$

where $2W$ is the well-known Debye–Waller factor calculated from the experimental temperature-dependent phonon density of states (DOS) (25, 39). The single and n-phonon scattering spectra are

$$A_1 = \frac{g(\varepsilon)}{\varepsilon}\langle n+1\rangle, \qquad \textbf{[S2]}$$

$$A_n = A_1 \circledast A_{n-1}. \qquad \textbf{[S3]}$$

The $g(\varepsilon)$ is the experimental phonon DOS (25), and n is the Planck distribution. We find that, even at temperatures >1,000 K, the contributions above the 5th multiphonon spectrum (S_5) are negligible. A global scaling factor ($b * S_{n>1}$) was applied to the total multiphonon scattering function throughout the Brillouin zone after folding to correct for normalization. The multiphonon scattering accounted for most of the background intensity as seen clearly in Fig. S1.

The correct alignment of the data in reciprocal space and multiphonon subtraction produced $S(q,\varepsilon)$ of high statistical quality. Thermal shifts of phonons reported previously, when available, were in good agreement (3, 19, 24).

Energy spectra at specific q points were evaluated by integrating over 0.0025 Å^{-3}. Phonon centroids were then fitted using the Levenberg–Marquardt nonlinear least square method for multiple skewed-Voigt functions. The skewed-Voigt functions gave the best fits to the known asymmetric lineshape of the ARCS time-of-flight spectrometer. Examples of the scattered intensities at a constant q, with fits, are shown for the X point in Fig. S2.

For comparison, a "slice" of unfolded 4D $S(q,\varepsilon)$ along a momentum direction is shown in Fig. S3. The data were processed using standard software and corrected for the phonon creation thermal factor (39, 52). First-principles calculations were performed using the s-TDEP method described in *Ab Initio Calculations* and elsewhere (17, 53). The experimental results are in good agreement with first-principles calculations throughout reciprocal space. There are benefits to assessing phonon intensities over multiple Brillouin zones, but these are not essential for a study of thermal expansion.

Ab Initio Calculations. Ab initio DFT calculations were performed with the projector augmented wave (54) formalism as implemented in VASP (41–43, 55). All calculations used a 5 × 5 × 5 supercell and a 500-eV plane wave energy cutoff. The Brillouin zone integrations used a 3 × 3 × 3 k-point grid, and the exchange–correlation energy was calculated with the AM05 functional (45–47). All calculations were converged to within 1 meV per atom. We found that calculations using other functionals as in refs. 56 and 57 gave similar phonon dispersion curves, and are expected to result in similar thermal trends.

Finite temperature phonon dispersions of silicon were calculated by fitting first-principles forces to a model Hamiltonian,

$$H = U_0 + \sum_i \frac{\mathbf{p}_i^2}{2m} + \frac{1}{2}\sum_{ij\alpha\beta}\Phi_{ij}^{\alpha\beta}u_i^\alpha u_j^\beta + \frac{1}{3!}\sum_{ijk\alpha\beta\gamma}\Phi_{ijk}^{\alpha\beta\gamma}u_i^\alpha u_j^\beta u_k^\gamma. \qquad \textbf{[S4]}$$

The forces on atoms were generated using DFT with various configurations of displaced atoms by a stochastic sampling of a canonical ensemble, with Cartesian displacements (u_i^α) normally distributed around the mean thermal displacement using

$$u_i^\alpha = \sum_k \frac{\epsilon_k^{i\alpha}c_k}{\sqrt{m_i}}\sqrt{-2\ln\xi_1}\sin(2\pi\xi_2). \qquad \textbf{[S5]}$$

The thermal factor, c_k, is based on thermal amplitudes of normal mode k, with eigenvector ϵ_k and frequency ω_k (33, 34, 58).

$$c_k = \sqrt{\frac{\hbar(2n_k+1)}{2\omega_k}}, \qquad \textbf{[S6]}$$

and ξ_1 and ξ_2 are stochastically sampled numbers between 0 and 1. The phonon distribution follows the Planck distribution, $n_k = (e^{\beta\hbar\omega_k}-1)^{-1}$, where the nuclear quantum effect can be turned off by taking the high-temperature limit of Eq. **S6**. The fitting to the model Hamiltonian used the TDEP method (17, 48). With thermal displacements from Eqs. **S5** and **S6**, we refer to our temperature-dependent calculations as the s-TDEP.

This method circumvents the issue of expensive computational resources required of ab initio molecular dynamics (AIMD), replacing AIMD with a Monte Carlo sampling of atomic positions and momentum near equilibrium positions (17, 33). The quasiharmonic model was calculated as described previously (25).

Phonon Shifts. The temperature-dependent renormalized phonon frequencies were calculated from the phonon self-energy. The phonon self-energy part, corrections to phonon energies from many-body interactions, comprises real and imaginary contributions,

$$\Sigma_\lambda = \Delta_\lambda + i\Gamma_\lambda. \qquad \textbf{[S7]}$$

Phonon scattering rates, and phonon lifetimes, are related to the imaginary part of the self-energy ($1/\tau_\lambda = 2\Gamma_\lambda$) for mode λ evaluated at the harmonic frequency. The imaginary part of the self-energy from many-body perturbation theory is

$$\Gamma_\lambda(\Omega) = \frac{\hbar\pi}{16}\sum_{\lambda'\lambda''}|\Phi_{\lambda\lambda'\lambda''}|^2 \times \left\{(n_{\lambda'}+n_{\lambda''}+1)\delta(\Omega-\omega_{\lambda'}-\omega_{\lambda''})+(n_{\lambda'}-n_{\lambda''}) \times [\delta(\Omega-\omega_{\lambda'}+\omega_{\lambda''})-\delta(\Omega+\omega_{\lambda'}-\omega_{\lambda''})]\right\}. \quad \text{[S8]}$$

The $\Omega(=E/\hbar)$ is the probing energy, and the delta functions conserve energy and momentum and sum over all possible three-phonon interactions between modes. The $\Phi_{\lambda\lambda'\lambda''}$ is the three-phonon matrix element, the Fourier transform of the third-order component of the interatomic potential (Eq. **S4**). The real part of the self-energy is calculated through a Kramers–Kronig transformation of the imaginary part,

$$\Delta(\Omega) = \frac{1}{\pi}\int d\omega \frac{\Gamma(\omega)}{\omega-\Omega}. \quad \text{[S9]}$$

The probing frequency, $\hbar\Omega$, is directly comparable to the renormalized frequencies from the harmonic energies with perturbative shifts calculated from the cubic term of the model Hamiltonian (34),

$$\hbar\Omega = \hbar(\omega_k + \Delta_k). \quad \text{[S10]}$$

Essentially, the effective potential method fits the stochastically sampled phonon potential to capture all even terms in the phonon potential as the "harmonic" frequencies (ω), and the odd-term contributions add shifts of the frequencies perturbatively (Δ) (31). This method includes higher-order phonon–phonon interactions by renormalizing terms in the model Hamiltonian.

Thermodynamic Calculations. Temperature-dependent coefficients of linear thermal expansion in silicon were calculated through the minimization of the free energy,

$$F(T,V) = E(T,V) + \sum_{\mathbf{q},k}\left(\frac{\hbar\omega_k(\mathbf{q},V,T)}{2} + k_B T\ln(1-e^{-\hbar\omega_k(\mathbf{q},T,V)/k_B T})\right), \quad \text{[S11]}$$

from quasiharmonic calculations, and from s-TDEP (Fig. 5). The QH assumes the only temperature dependence of the entropy is from the volume expansion $\varepsilon_k(V\{T\})$ and the Planck distribution (n_k), whereas the anharmonic s-TDEP method minimizes the free energy for temperature and volume simultaneously. The vibrational entropy from all phonon modes, $\sum_k$, was calculated as (1)

$$S_{\text{vib}}(T) = 3k_B\sum_k\left[(n_k+1)\ln(n_k+1) - n_k\ln(n_k)\right]. \quad \text{[S12]}$$

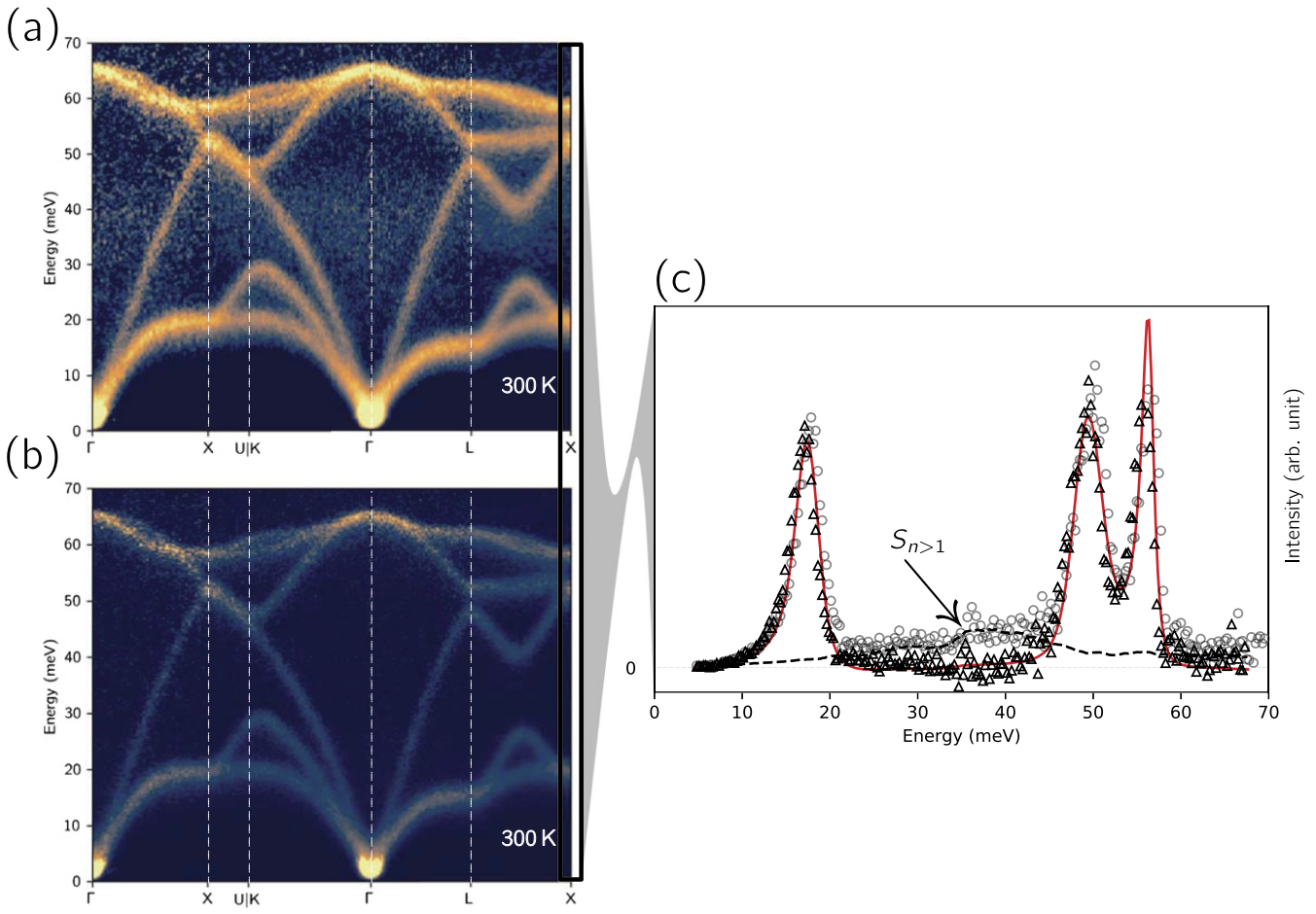

Fig. S1. Folded inelastic neutron scattering data (*A*) without and (*B*) with multiphonon subtracted $S(q,\varepsilon)$ at 300 K. (*C*) Scattering intensity and fitted spectrum at the *X* point. Fitted peaks are shown as the red solid line. Gray circles are without (from *A*) and black triangles are with (from *B*) multiphonon scattering subtracted. Black dashed line shows subtracted multiphonon scattering intensity.

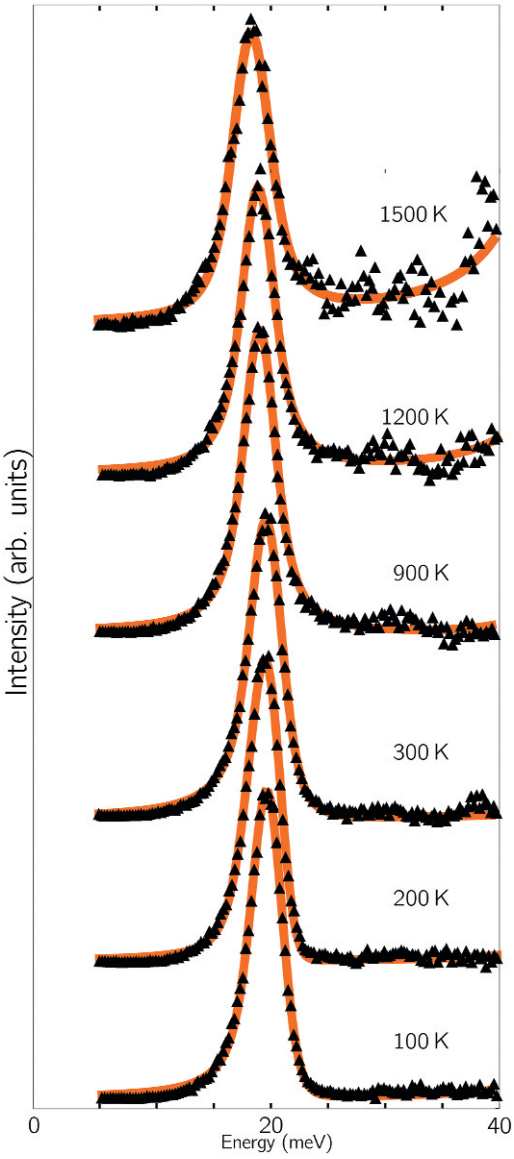

Fig. S2. Constant q-$S(q,\varepsilon)$ data at the X point for 100, 200, 300, 900, 1,200, and 1,500 K. Data are black markers, and fits are in orange.

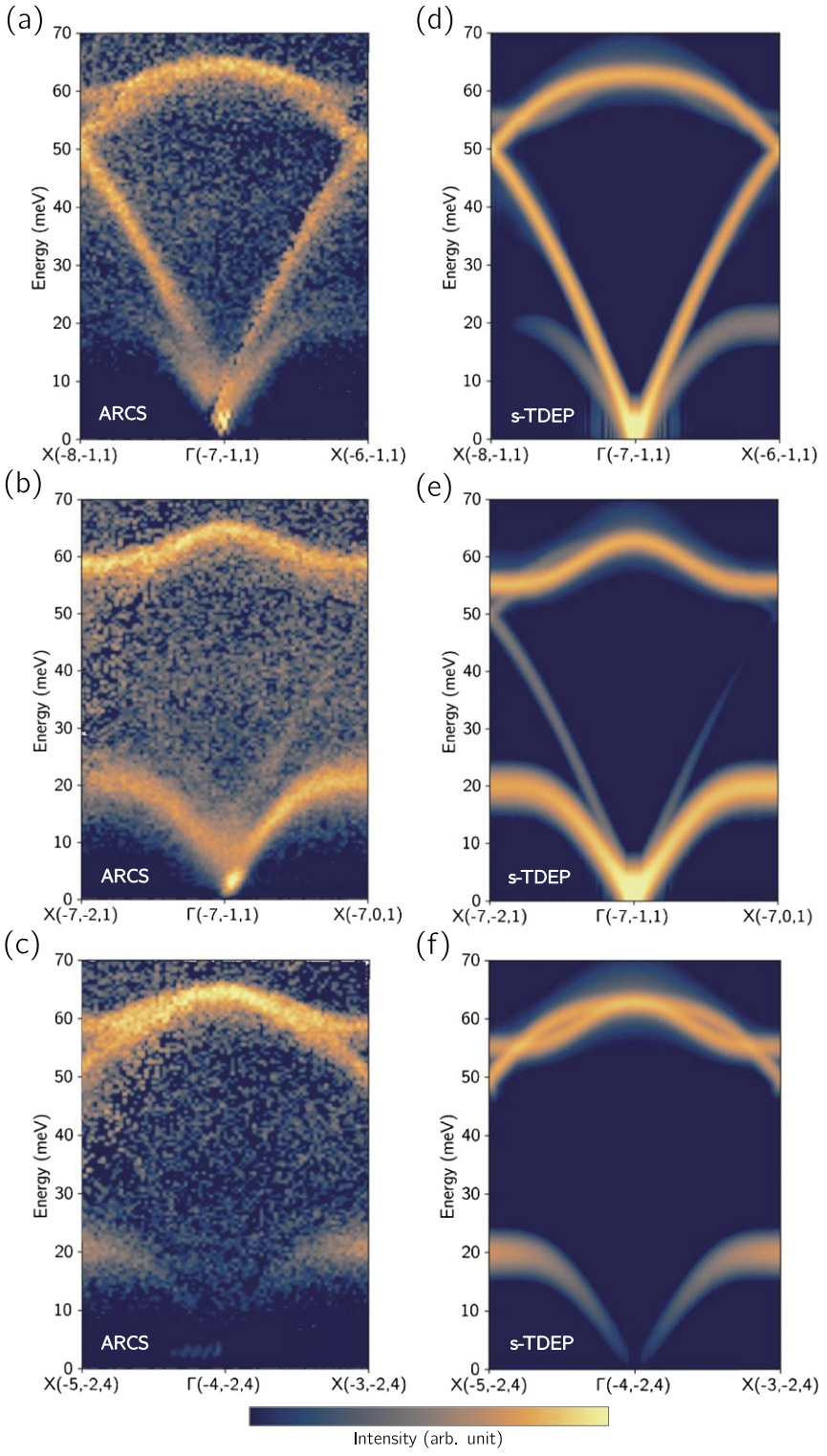

Fig. S3. (*A*–*C*) Inelastic neutron scattering and (*D*–*F*) first-principles calculations of $S(q,\varepsilon)$ at 300 K along momenta q (X–Γ–X) in different Brillouin zones. Calculated $S(q,\varepsilon)$ was corrected for instrument resolution and polarization effects to match the experiment conditions (38, 39).